

Flow and heat transfer of nanofluids in a cylindrical permeable wavy channel embedded in porous medium using Buongiorno's model

D. N. Dash*, K. S. Arjun†, D. N. Thatoi*, Rifaqat Ali‡, M. K. Nayak * and Ali J. Chamkha§

*Department of Mechanical Engineering,
Faculty of Engineering and Technology,
Institute of Technical Education and Research,
Siksha 'O' Anusandhan (Deemed to be University),
Bhubaneswar 751030, Odisha, India

†Division of Mechanical Engineering, School of Engineering,
Cochin University of Science and Technology, Kalamassery 682022,
Kerala, India

‡Department of Mathematics,
College of Science and Arts at Muhayil,
King Khalid University, 61413 Abha, Saudi Arabia

§Faculty of Engineering,
Kuwait College of Science and Technology,
Doha District, Kuwait
✉mkn2122@gmail.com

Received 20 June 2023

Revised 3 October 2023

Accepted 5 November 2023

Published 8 January 2024

This investigation deals with the flow of Al_2O_3 -water nanofluid in a wavy porous channel embedded in porous rocks. Fluid exchange takes place uniformly between porous rocks and the wavy channel. In this analysis, cylindrical and parallel plate wavy porous channels are considered. Consequences of Brownian motion and thermophoresis on the flow inside a wavy porous channel are elucidated. The modeled equations are made dimensionless by using dimensionless quantities. Impacts of flow parameters on the velocity, temperature, Nusselt number and friction factor are depicted through graphs. The numerical results with respect to parallel plate wavy porous channel are validated by comparing with the published results. The effectiveness of the cylindrical wavy porous channel as a heat transfer enhancement device in comparison to the parallel plate wavy porous channel is confirmed in this study. Designing devices at microlevels and understanding the heat transfer enhancement mechanism in wavy channels using the nanoparticle addition are the major outcomes from the results of this numerical investigation. The heat and mass transfer rate enhancements in the wavy porous channels are due to the

✉Corresponding author.

higher Brownian motion in the boundary layer region and accelerated thermophoresis through thermal and concentration boundary layer thicknesses.

Keywords: Wavy porous channel; Buongiorno's model; heat transfer; nanofluid.

1. Introduction

It is a fact that the low heat transfer (HT) qualities of base fluids like water, mineral oils and ethylene glycol make it difficult to increase the effectiveness of many thermal systems. Some solids, including metals, have substantially greater thermal conductivities than typical liquids. As a result, adding a suspension of tiny solid particles to pure liquids works well to improve the liquids' ability to transmit heat. A particle between 1 nm and 100 nm in size is referred to as a nanoparticle. The stable and uniform suspension of solid particles in a base fluid, known as a nanofluid, improves the thermal and rheological behaviors of the fluid without affecting its chemical or physical properties. Choi¹ pioneered the idea of suspending nanoparticles in regular fluids to improve heat transfer. In addition to having better thermal conductivity, adding nanoparticles to fluids rather than micro-particles is done for a variety of scientific reasons, including increased stability, less erosion and clogging and a reduced need for powerful pumping. There are several potential and practical physical uses for nanofluids. Nanofluids, for instance, are used in a variety of industries, such as biomedicine, automotive cooling systems, fuel cells, solid-state lighting, microelectronics, microchips, food processing, shipping and manufacturing. Metals, metallic oxides and carbon nanotubes are used in inclusion for biomedical equipment, lubrication and heat transmission.² The consequences of introducing nanoparticles to base fluid have been the subject of several researches recently, with a particular emphasis on the ensuing thermal characteristics. For instance, Rehman *et al.*³ analyzed silver–water and silver–blood base nanofluids flow over fluctuating disk with the influence of viscous dissipation over the fluctuating disk. Rehman *et al.*⁴ further analyzed graphene oxide–ethylene glycol and graphene oxide–blood base nanofluids flow over a vertical surface. It is seen that the velocity profile is slowed down as the stretching parameter and nanoparticle volume percentage are increased. Ahmed⁵ explored the temperature-dependent viscosity effect on forced convective $\text{CH}_3\text{OH}\text{--Fe}_3\text{O}_4$ nanofluid flow through annular duct. Haider *et al.*⁶ studied on the impact of heat transfer on peristaltic flow of nanofluid and its applications in real-world problems. Hammid *et al.*⁷ carried out laminar rarefied flow analysis in a microchannel with $\text{H}_2\text{O}\text{--Cu}$ nanofluid. They discovered that, while the Nusselt number rises with greater nanoparticle volume fractions, the nanoparticle volume fraction has no effect on the velocity distribution or temperature field. The works in the related areas are observed in Refs. 8–11.

Due to the extensive range of applications in industry and engineering heat transfer, internal flows attracted the researchers toward them. The flow through channels of various cross-sections gained the attention of many researchers and

engineers due to advantages in nuclear power plant, solar cells and several thermal systems. A comprehended pattern of flow in wavy channel (WC) with penetrable walls is one of the trending areas of research. Plenty of research works have been done in this aspect. Simulation of Cu–water nanofluid through a WC has been investigated by Ahmed *et al.*¹² The solutions are computed via the finite difference method. In their study, incremented amplitude of WC upgrades the Nusselt number significantly. Lin *et al.*¹³ developed a model to describe the thermal performance in a WC by means of wavelength and amplitude. Interaction between liquid and solid particles in a finite symmetric WC has been described by Ijaz *et al.*¹⁴ It is remarked that velocity field diminishes for higher electro-osmotic parameter. Flow inside a WC has been examined by Rasoulzadeh and Panfilov¹⁵ employing perturbation method. It is established that cubic corrections exist in the case of impermeable walls. Vo *et al.*¹⁶ evaluated the flow of γ -AlOOH nanoliquid in a sinusoidal WC. It is remarked that improving the percentage of nanoadditives yields higher Nusselt number. Experimental study on nanofluid flow in a microchannel heat sink consisting of WC has been done by Sajid *et al.*¹⁷ They demonstrated that channel wavelength has a positive impact on heat transfer rate (HTR). Sadeghi *et al.*¹⁸ analyzed the thermal behavior of magnetic buoyancy-driven flow in ferrofluid-filled wavy enclosure furnished with two circular cylinders.

The porous channel has emerged as a potential solution because of its pore–solid structural orientation as it enables a higher rate of heat transfer with comparatively less pressure loss. Additionally, the heat transfer rate may be greatly increased by using nanofluid in place of regular fluid. Hajipour and Dehkordi¹⁹ undertook both analytical and numerical approaches to dissect heat transfer inside a channel. They considered a channel filled (partially) with porous medium. They obtained that Nusselt number enhances at lower cold wall of the channel due to the accumulation of nanoparticles' mass flux. Reddy and Bhargavi²⁰ employed Darcy–Brinkman model to scrutinize the flow through parallel plates. Sheremet *et al.*²¹ considered the Forchheimer–Buongiorno approach to evaluate the flow through a wavy cavity. Turkyilmazoglu²² had examined the wall-driven flow of nanofluid in a channel by means of Buongiorno's model.

Researches on flow and heat transfer in porous WCs with the height of wall waviness as half the radius length, addressing the turbulent nanofluid flow, are not yet available in the literature. The main aim of this work is to extend the knowledge of heat transfer and hydrodynamics of Al_2O_3 –water nanofluid in cylindrical and parallel plate permeable wavy channels embedded in porous rocks. Apart from the exploration of disparate parametric effects, the effects of thermophoresis and Brownian motion on thermal enhancement are given special attention. The effects of uniform heat flux at the boundary are taken into account. The obtained outcomes are visualized through graphs. A systematic comparison of CFD prediction of forced convection of Al_2O_3 –water nanofluid is presented. The major geometrical criterion of the height of wall waviness is considered in this

forced convection study of wavy porous channels, which was missing in majority of the previous studies.

2. Numerical Simulation and Boundary Conditions

ANSYS Fluent 15.0²³ is used for the numerical simulation of Al₂O₃–water nanofluid flow, employing the finite volume method. The flow is assumed 2D, steady, axisymmetric and incompressible with constant properties and neglecting the gravity effect. The model used for turbulence is the Shear Stress Transport *k*– ω model²⁴ in this investigation. The channel entrance treated as calming section is assigned constant temperature and uniform velocity. The flow domain is bounded with slip walls, calming wall sections are specified as adiabatic and permeable wavy walls are provided with uniform and constant 5000-W/m² heat flux. The nanofluid is at 300 K and the width of the parallel plate wavy porous channel is 15 cm. Also, 25 cm is the length of each calming length section and the total channel length is 200 cm. The wavy wall temperature is 310 K.

2.1. Cylindrical wavy channel

We assume the flow of Al₂O₃–water nanofluid in cylindrical wavy porous channel (Fig. 1). Figure 1 illustrates the geometry of cylindrical wavy porous channel with $0 < R < R_\omega \Omega(X)$, $0 < X < L$ and $0 < \theta < 2\pi$, in which $\Omega(X)$ may be a periodical function with period l and average amount 1. We consider $\Omega(0) = 1$ at the channel's inlet. When $\Omega(X) = 1$, the channel becomes a normal cylinder. Let R_ω and L be the mean radius and characteristic length of the cylindrical channel. It is assumed that the influx at channel's inlet at $X = 0$ is W_0 .

The boundary condition on the inlet of channel imposing the average velocity U_0 (or flow rate W_0) is

$$U_0 = \frac{2}{[R_\omega \Omega(0)]^2} \int_0^{R_\omega \Omega(0)} U_X(R, 0) R dR. \quad (1)$$

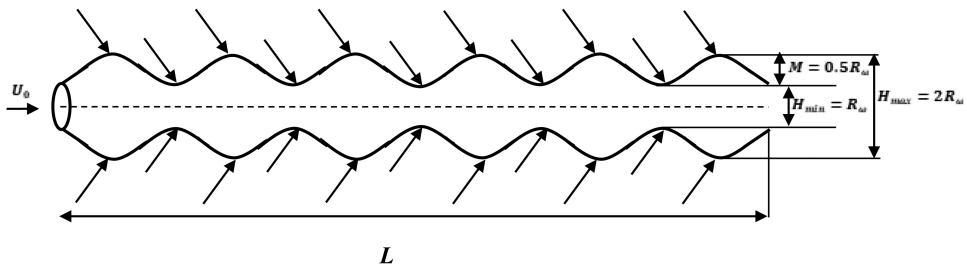


Fig. 1. Schematic of the cylindrical wavy porous channel problem: U_0 (average velocity of the channel), M (half the radius) = $0.5R_\omega$ (mean radius of the cylindrical channel), H_{\min} (minimum of channel height) = R_ω and H_{\max} (maximum of channel height) = $2R_\omega$.

We consider the appropriate parameters as

$$\left. \begin{aligned} x &= \frac{X}{L}, & r &= \frac{R}{R_\omega}, & p &= \frac{P}{p_0}, & u &= \frac{U_X}{U_0}, \\ v &= \frac{U_R}{U_0}, & \omega &= \frac{R_\omega}{L}, & \varepsilon &= \frac{l}{L}, & \text{Re} &= \frac{\rho_f U_0 R_\omega}{\mu_f} \end{aligned} \right\} \quad (2)$$

where P, U_X and U_R are the pressure, axial fluid velocity and radial fluid velocity, respectively. Further, p, u and v are the dimensionless pressure, dimensionless axial velocity and dimensionless radial velocity, respectively. The characteristic pressure p_0 is determined as the pressure drop along the length L caused by Poiseuille's flow at velocity U_0 : $p_0 = \frac{\mu U_0 L}{R_\omega^2}$.

Let the parameters ω and ε be so small that $0 < \omega, \varepsilon \ll 1$. In this case, the ratio $\frac{\omega}{\varepsilon}$ accounts for the various flow regimes. Channels having straight walls are the limiting cases:

- When $\frac{\omega}{\varepsilon} \gg 1$, the channel's aperture may be very large, and the associated corrugations could be ignored.
- When $\frac{\omega}{\varepsilon} \ll 1$, the corrugation period becomes very large.

Here, we consider the case when $\omega \sim \varepsilon^{\alpha^*}$, $\alpha^* \sim 1$ (Fig. 1).

The thermophysical properties of nanofluid are

$$\mu_{\text{nf}} = \frac{\mu_f}{1 - 34.87 \left(\frac{d_p}{d_f}\right)^{-0.3} \phi^{1.03}}, \quad (3)$$

$$\rho_{\text{nf}} = (1 - \phi)\rho_f + \phi\rho_p, \quad (4)$$

$$(\rho c_p)_{\text{nf}} = (1 - \phi)(\rho c_p)_f + \phi(\rho c_p)_p, \quad (5)$$

$$k_{\text{nf}} = k_f \left[1 + 4.4(\text{Re})^{0.4} \text{Pr}^{0.66} \left(\frac{T}{T_{fr}}\right)^{10} \left(\frac{k_p}{k_f}\right)^{0.03} \phi^{0.66} \right], \quad (6)$$

$$\text{Re} = \frac{\rho_f u_B d_p}{\mu_f}, \quad (7)$$

$$u_B = \frac{2k_B T}{\pi \mu_f d_p^2}, \quad (8)$$

where $\mu_{\text{nf}}, \rho_{\text{nf}}, (\rho c_p)_{\text{nf}}$ and k_{nf} are, respectively, the dynamic viscosity, density, specific heat capacity and thermal conductivity of nanofluid. Further, $\mu_f, \rho_f, (\rho c_p)_f$ and k_f are, respectively, the dynamic viscosity, density, specific heat capacity and thermal conductivity of base fluid. In addition, $\rho_p, (\rho c_p)_p$ and k_p are, respectively, the density, specific heat capacity, thermal conductivity and diameter of the nanoparticle. Here, d_f and d_p are the diameters of base fluid molecule and nanoparticle, respectively, ϕ is the solid volume fraction, T_{fr} is the freezing point of base fluid, k_B ($= 1.38064 \times 10^{-23} \text{J/K}$) is the Boltzmann constant, T is the temperature and u_B is

the nanoparticle Brownian velocity. Here, for water, $d_f = 0.385$ nm. Also, Pr is the Prandtl number and Re is the Reynolds number.

Accordingly, the dimensionless governing equations are

$$\omega \frac{\partial u}{\partial x} + \frac{1}{r} \frac{\partial(rv)}{\partial r} = 0, \tag{9}$$

$$\text{Re} \left(\omega u \frac{\partial u}{\partial x} + v \frac{\partial u}{\partial r} \right) = -\frac{\partial p}{\partial x} + \frac{\mu_{\text{nf}}}{\mu_f} \frac{\rho_f}{\rho_{\text{nf}}} \left[\omega^2 \frac{\partial^2 u}{\partial x^2} + \frac{1}{r} \frac{\partial}{\partial r} \left(r \frac{\partial u}{\partial r} \right) \right], \tag{10}$$

$$\text{Re} \left(\omega u \frac{\partial v}{\partial x} + r \frac{\partial v}{\partial r} \right) = -\frac{1}{r} \frac{\partial p}{\partial r} + \frac{\mu_{\text{nf}}}{\mu_f} \frac{\rho_f}{\rho_{\text{nf}}} \left[\omega^2 \frac{\partial^2 v}{\partial x^2} + \frac{1}{r} \frac{\partial}{\partial r} \left(r \frac{\partial v}{\partial r} \right) \right], \tag{11}$$

$$\begin{aligned} \text{Pr Re} \left(\omega u \frac{\partial \theta}{\partial x} + v \frac{\partial \theta}{\partial r} \right) &= \frac{\alpha_{\text{nf}}}{\alpha_f} \left[\frac{\partial^2 \theta}{\partial r^2} + \frac{1}{r} \left(\frac{\partial \theta}{\partial r} \right) \right] \\ &+ \text{Pr} \left(\frac{(\rho c_p)_f}{(\rho c_p)_{\text{nf}}} \right) \left[\text{Nb} \frac{\partial \theta}{\partial r} \frac{\partial \phi}{\partial r} + \text{Nt} \left(\frac{\partial \theta}{\partial r} \right)^2 \right], \end{aligned} \tag{12}$$

$$\text{Le Pr Re} \left(\omega u \frac{\partial \phi}{\partial x} + v \frac{\partial \phi}{\partial r} \right) = \left[\frac{\partial^2 \phi}{\partial r^2} + \frac{1}{r} \left(\frac{\partial \phi}{\partial r} \right) \right] + \frac{\text{Nt}}{\text{Nb}} \left[\frac{\partial^2 \theta}{\partial r^2} + \frac{1}{r} \frac{\partial \theta}{\partial r} \right]. \tag{13}$$

The dimensionless boundary conditions are

$$\left. \begin{aligned} 1 &= 2 \int_0^{\Omega(0)} ru(r, 0) dr = 2 \int_0^1 ru(r, 0) dr, \\ \left(\frac{\partial u}{\partial r} \right)_{r=0} &= 0, \quad (v)_{r=0} = 0, \quad (\theta)_{r=0} = 1, \quad (\phi)_{r=0} = 1, \\ (u)_{r=\Omega(x)} &= \omega u^*, \quad (v)_{r=\Omega(x)} = -\omega v^*, \quad (\theta)_{r=\Omega(x)} = 0, \quad (\phi)_{r=\Omega(x)} = 0. \end{aligned} \right\} \tag{14}$$

Here, $\omega u^* = \frac{U_X^*}{U_0}$ and $\omega v^* = \frac{U_B^*}{U_0}$ are the two components of velocity of fluid flow through channel's boundary, α_{nf} and α_f are, respectively, the thermal diffusivities of nanofluid and base fluid, θ is the nondimensional temperature, Nb is the Brownian motion parameter, Nt is the thermophoresis parameter and Le is the Lewis number.

2.2. Parallel plate wavy channel

The approach followed in Sec. 2.1 has been applied to study the flow of Al_2O_3 -water nanofluid in a slab-shaped parallel plane wavy channel with penetrable walls embedded in porous rocks (Fig. 2). As the depth of the channel normal to the flow direction is infinite, the problem is considered as two-dimensional (Fig. 2). The thermophysical properties of water and nanoparticles at $T = 300$ K as shown in Table 1.

The boundary condition at the inlet section with average velocity U_0 is

$$U_0 = \frac{1}{H\Omega(0)} \int_0^{H\Omega(0)} U_X(0, Z) dZ. \tag{15}$$

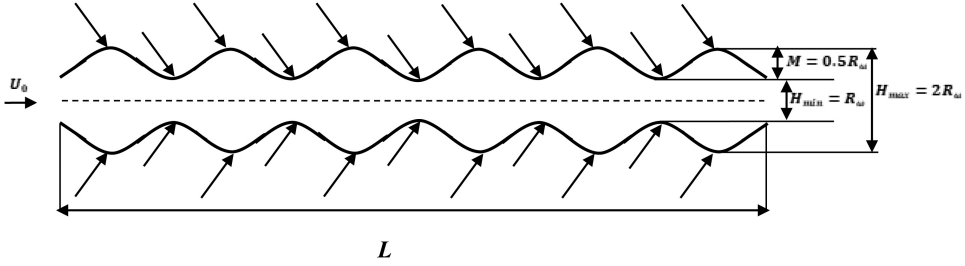


Fig. 2. Schematic of the parallel plate wavy porous channel problem: U_0 (average velocity of the channel), M (half the radius) = $0.5R_w$ (mean radius of the cylindrical channel), H_{\min} (minimum of channel height) = R_w and H_{\max} (maximum of channel height) = $2R_w$.

It is assumed that the influx from host porous rocks is uniform with (U_X^*, U_Z^*) . Let us introduce the following dimensionless variables:

$$\left. \begin{aligned} x &= \frac{X}{L}, & z &= \frac{Z}{H}, & u &= \frac{U_X}{U_0}, \\ v &= \frac{U_Z}{U_0}, & p &= \frac{P}{p_0}, \end{aligned} \right\} \quad (16)$$

with $p_0 = \frac{\mu U_0 L}{H^2}$, $Re = \frac{\rho U_0 H}{\mu}$ and $w = \frac{H}{L}$.

Using the above assumptions, the dimensionless governing equations of the steady-state incompressible flow are

$$\omega \frac{\partial u}{\partial x} + \frac{\partial v}{\partial z} = 0, \quad (17)$$

$$Re \left(\omega u \frac{\partial u}{\partial x} + v \frac{\partial u}{\partial z} \right) = -\frac{\partial p}{\partial x} + \frac{\mu_{nf}}{\mu_f} \frac{\rho_f}{\rho_{nf}} \left[\omega^2 \frac{\partial^2 u}{\partial x^2} + \frac{\partial^2 u}{\partial z^2} \right], \quad (18)$$

$$Re \left(\omega u \frac{\partial v}{\partial x} + v \frac{\partial v}{\partial z} \right) = -\frac{1}{\omega} \frac{\partial p}{\partial z} + \frac{\mu_{nf}}{\mu_f} \frac{\rho_f}{\rho_{nf}} \left[\omega^2 \frac{\partial^2 v}{\partial x^2} + \frac{\partial^2 v}{\partial z^2} \right], \quad (19)$$

$$\begin{aligned} Pr Re \left(\omega u \frac{\partial \theta}{\partial x} + v \frac{\partial \theta}{\partial z} \right) &= \frac{\alpha_{nf}}{\alpha_f} \left[\omega^2 \frac{\partial^2 \theta}{\partial x^2} + \frac{\partial^2 \theta}{\partial z^2} \right] \\ &+ Pr \left[Nb \left(\omega^2 \frac{\partial \phi}{\partial x} \frac{\partial \theta}{\partial x} + \frac{\partial \phi}{\partial z} \frac{\partial \theta}{\partial z} \right) \right. \\ &\quad \left. + Nt \left\{ \omega^2 \left(\frac{\partial \theta}{\partial x} \right)^2 + \left(\frac{\partial \theta}{\partial z} \right)^2 \right\} \right] + \frac{(\rho c_p)_f}{(\rho c_p)_{nf}} Q \theta, \quad (20) \end{aligned}$$

$$Le Pr Re \left(\omega u \frac{\partial \phi}{\partial x} + v \frac{\partial \phi}{\partial z} \right) = \left[\omega^2 \frac{\partial^2 \phi}{\partial x^2} + \frac{\partial^2 \phi}{\partial z^2} \right] + \frac{Nt}{Nb} \left(\omega^2 \frac{\partial^2 \theta}{\partial x^2} + \frac{\partial^2 \phi}{\partial z^2} \right). \quad (21)$$

Table 1. Thermophysical properties of water and nanoparticles at $T = 300\text{ K}$.²⁵

Material	ρ (kg/m ³)	k (W/mk)	c_p (J/kgK)	μ ($\times 10^6$ kg/ms)	d_p (nm)
Al ₂ O ₃	3970	40	765	—	33
Water	993	0.628	4178	695	—

The resulting boundary conditions are

$$\left. \begin{aligned} \frac{1}{2} &= \int_0^{\Omega(0)} u(0, z) dz = \int_0^{\frac{1}{2}} u(0, z) dz, \\ \left(\frac{\partial u}{\partial z} \right)_{z=0} &= 0, \quad (v)_{z=0} = 0, \quad (\theta)_{z=0} = 1, \quad (\phi)_{z=0} = 1, \\ (u)_{z=\Omega(x)} &= \omega u^*, \quad (v)_{z=\Omega(x)} = -\omega v^*, \quad (\theta)_{z=\Omega(x)} = 0, \quad (\phi)_{z=\Omega(x)} = 0. \end{aligned} \right\} \quad (22)$$

3. Mesh Independency and Validation

Diffusion and convection equations are discretized with central differencing and second-order upwind methods. For domain discretization, a structured, quadrilateral and nonorthogonal mesh, more refined near the wavy surfaces (Figs. 3 and 4), is used to find out the minor changes accurately ($y < 1$) in the gradients of velocity and temperature. SIMPLE algorithm for pressure–velocity coupling and second-order implicit scheme for transient formulation were employed. Simulations were run to achieve stable statistics of the flow and turbulence and iterations were continued until the convergence reached the residual value of 1×10^{-5} for every variable. Mesh independency studies included four ranges of mesh sizes. The height H_{\min} is taken as the radius and height H_{\max} is taken as the diameter of the cylindrical wavy channel (2.5 cm) and height for the parallel plate wavy channel is taken as $M =$ half the radius at $Re = 5000$ and $\phi = 4\%$. For the mesh sizes $70 \times 700, 80 \times 800, 90 \times 900$ and 100×1000 , the Nu values obtained are 50.32, 52.26, 53.75 and 53.77, and the friction factors obtained are 0.0366, 0.0337, 0.0316 and 0.0315, respectively. The mesh size (100×1000) provides enough accuracy.

The comparison of the results of parallel plate wavy channel on the basis of the values of Nu/Nu_0 ratio in respect of Ref. 26 is plotted in Fig. 5 as functions of Re

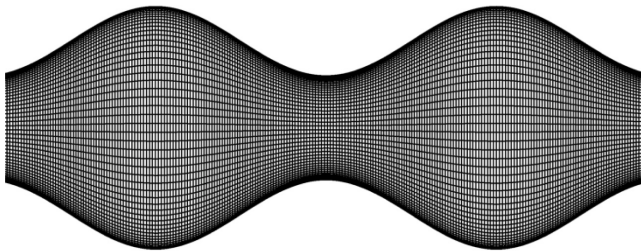


Fig. 3. Mesh for the cylindrical wavy channel domain.

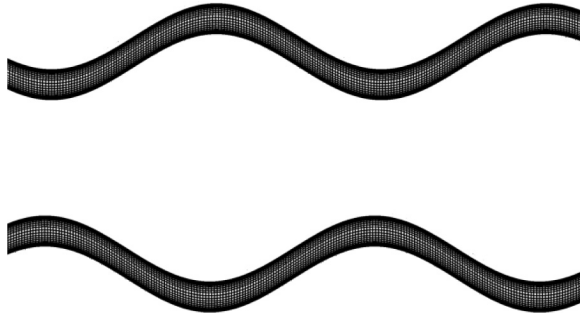


Fig. 4. Mesh for the parallel plate wavy channel domain (magnified view).

for a fixed geometry (height of the wall waviness in relation to the total height of the channel, $M = 0.2$ and distance between the wavy wall and flat wall, $H_{\max} = 1$). Parametric experimental results describing the waviness factor are not available with respect to any of the wavy channels used in this study. The results obtained for the above geometry using the solver used in this study are used for comparison of Nusselt number with that of its base fluid as a ratio. The published and our study values on Nusselt number ratio were almost similar with $R^2 = 0.999$, validating the model reliability.

4. Results and Discussion

In this section, the effects of distinct flow parameters on velocity, temperature, Nusselt number and friction factor are discussed with the help of graphs. Here, we considered the flow of Al_2O_3 -water nanofluid through distinct cross-section. One is the symmetric cylindrical channel and another is parallel plate channel with permeable wavy walls embedded in porous medium.

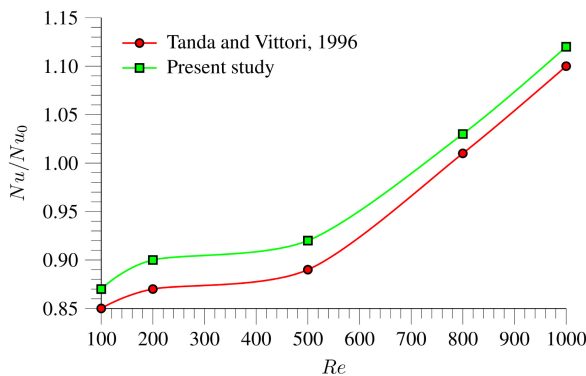


Fig. 5. (Color online) Validation of nanofluid-to-base fluid Nusselt number ratio in parallel plate wavy porous channel with the results of Ref. 26.

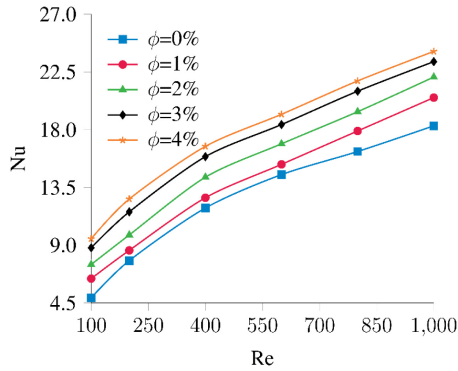


Fig. 6. (Color online) Consequences of ϕ and Re below 1000 on the Nusselt number for cylindrical channel.

The Nusselt number values are depicted as a function of Reynolds number Re (Re = 100–10000) by varying the Prandtl number Pr (1.4–8.69) and volume fraction (0–4%) of nanoparticles (Figs. 6–11). Both ϕ (Figs. 6–9) and Pr (Figs. 10 and 11) enhance the heat transfer. As Pr increases the thermal boundary layer thickness diminishes, which leads to high heat transfer. The Nusselt number enhancements for cylindrical wavy channels were 4.92 and 6.52 times with Pr and ϕ variables, respectively, for the Re of 100–1000 in this study. For Pr, the enhancement was up to 18.02 times for Reynolds number Re (Re = 100–10000). Rate of heat transfer rises by 16.4 times (4.29 times only when considering the increase in Re up to 1000 and 6.66 times, respectively, for parallel plate wavy channels in this study). The perturbation was significant with the mid-height horizontal velocity with respect to the variation of Pr in this study. A very small quantity of nanoparticle addition can ensure an enhancement in heat transfer through higher thermal conductivity and higher velocity gradient. Low temperature gradient, thin momentum and thick

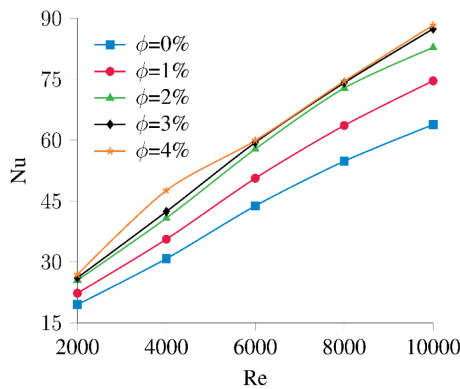


Fig. 7. (Color online) Consequences of ϕ and Re above 1000 on the Nusselt number for cylindrical channel.

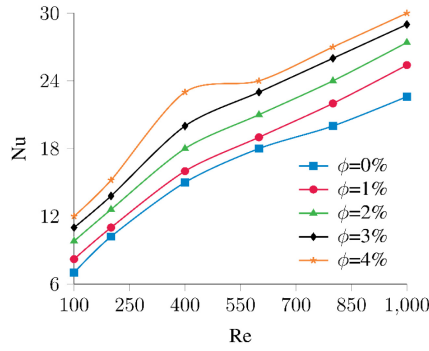


Fig. 8. (Color online) Consequences of ϕ and Re below 1000 on the Nusselt number for parallel plate channel.

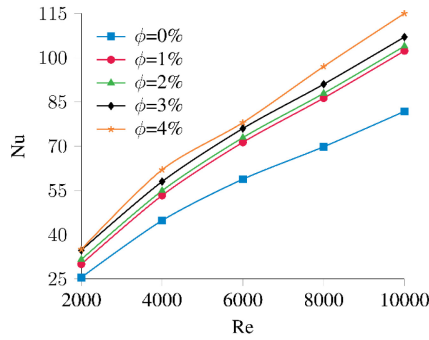


Fig. 9. (Color online) Consequences of ϕ and Re above 1000 on the Nusselt number for parallel plate channel.

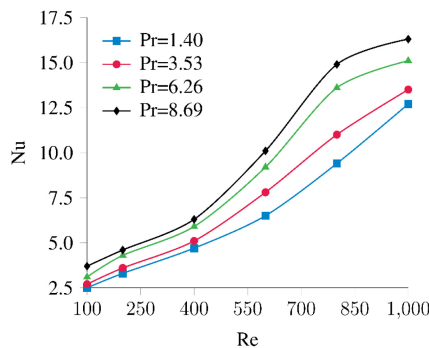


Fig. 10. (Color online) Consequences of Pr on the Nusselt number for cylindrical channel.

thermal boundary layers augment in this achievement. Bulk fluid and boundary temperatures justify the reduction in thermophoresis owing to the addition of nanoparticles. But Brownian motion at this condition creates an oscillatory behavior due to the action of base fluid's higher thermal diffusivity. Though Pr reduces

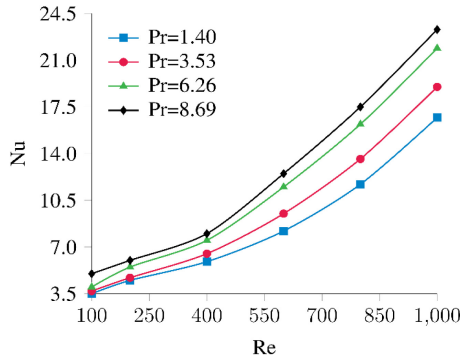


Fig. 11. (Color online) Consequences of Pr on the Nusselt number for parallel plate channel.

concentration, it increases temperature with the distribution, mostly by convection as momentum diffusivity takes domination over thermal diffusivity.

Reduction in friction factor and enhancement in shear stress with Re are more evident at higher Re (Figs. 12 and 13). Cylindrical wavy channel has greater friction factor compared to parallel plate channel. Brownian motion leads to pressure drop enhancement for nanofluids than regular fluids, nullifying the effect of thermophoresis. The quantification of these variations decides the design as well as running costs. Induction of reduced thickness of momentum boundary layer and friction factor with enhancement in shear rate is the effect of nanoparticle addition. Wavy surfaces show higher turbulence than straight surfaces at higher Re.

The mean difference temperature between the bulk and wall base temperatures define LMTD (log mean temperature difference). As the Al_2O_3 -water nanofluid showed less wall base temperature (90.42% reduction for cylindrical wavy channel and 90.51% reduction for parallel plate wavy channel) due to higher thermal conductivity and heat absorbing capacity (Figs. 14 and 15), lower LMTD (5.74% reduction for cylindrical wavy channel and 6.23% reduction for parallel plate wavy channel) is obtained corresponding to all Re values of nanofluids (Figs. 16 and 17)

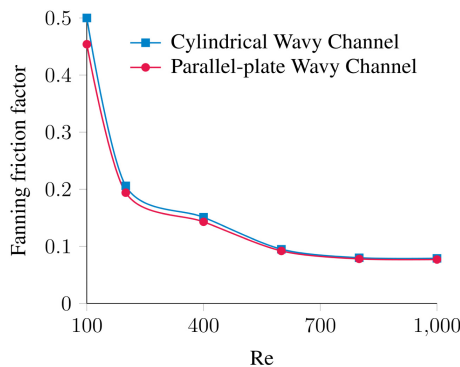


Fig. 12. (Color online) Consequences of Re below 1000 on the fanning friction factor.

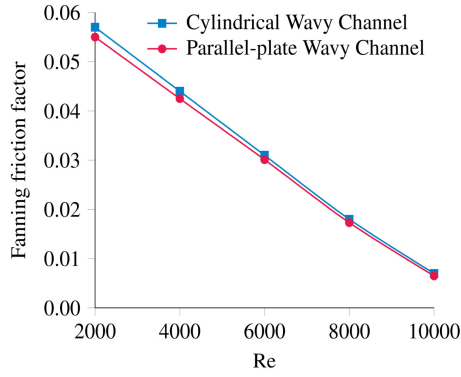


Fig. 13. (Color online) Consequences of Re above 1000 on the fanning friction factor.

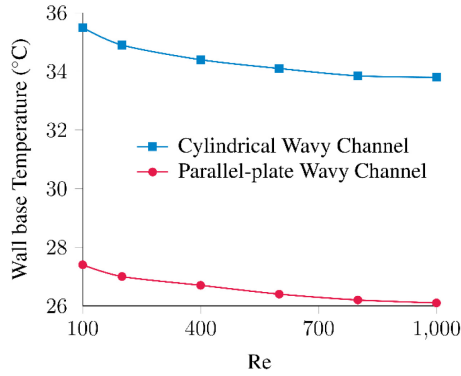


Fig. 14. (Color online) Consequences of Re below 1000 on the wall base temperature.

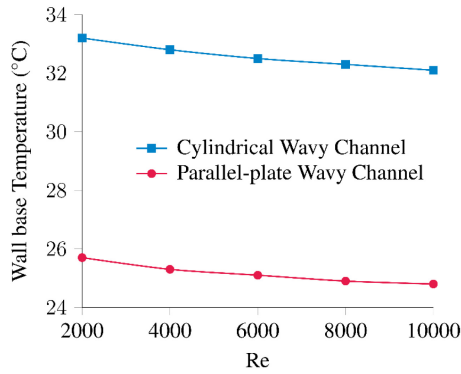


Fig. 15. (Color online) Consequences of Re above 1000 on the wall base temperature.

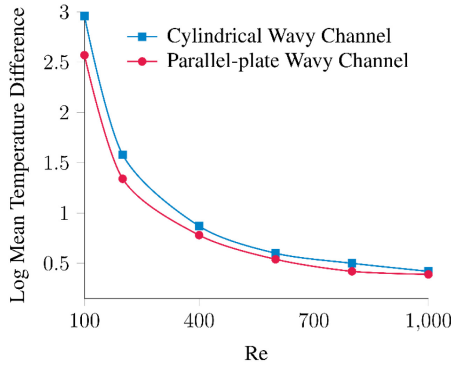


Fig. 16. (Color online) Consequences of Re below 1000 on the log mean temperature difference.

investigated. Thermal resistance (LMTD/heat transfer rate) decreases with rising nanoparticle volume fraction and Re due to the convective heat transfer coefficient enhancement. It is seen that cylindrical wavy channel has higher temperature difference than parallel plate wavy channel. It is demonstrated that cylindrical wavy channel exhibits larger temperature at the wall.

The mean bulk temperatures of the nanofluid inside the wavy channel for the effects of Re and Pr are displayed in Figs. 18 and 19. Rising Prandtl number belittles the average bulk fluid temperature (30% reduction for cylindrical wavy channel and 29.2% reduction for parallel plate wavy channel). Enhancement in forced convection and consequent fluid heat transfer reduces the mean bulk temperature with Re. This is due to the fact that, when Pr gets larger, viscous diffusion increases which results in lower thermal boundary layer thickness. Hence the temperature decreases.

The low viscosity makes the nanofluid temperature equal to that of the heated wall very quickly at low Pr. Peaks of flow are observed with the rise in Pr, consequent to slow reduction in fluid temperature at the boundary walls and channel outlet. This causes formation and thickening of thermal boundary layer at heated wall and an

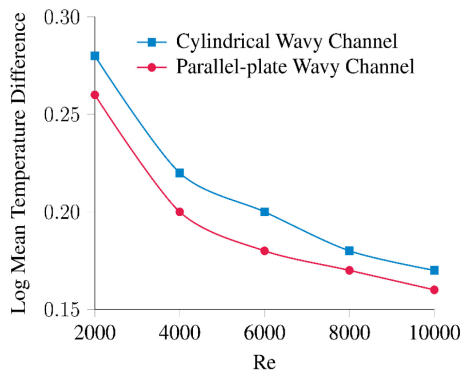


Fig. 17. (Color online) Consequences of Re above 1000 on the log mean temperature difference.

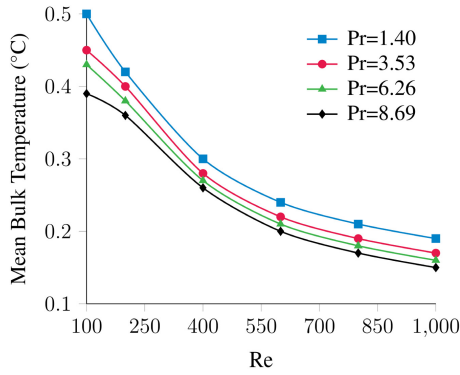


Fig. 18. (Color online) Consequences of Pr on the mean bulk temperature for cylindrical channel.

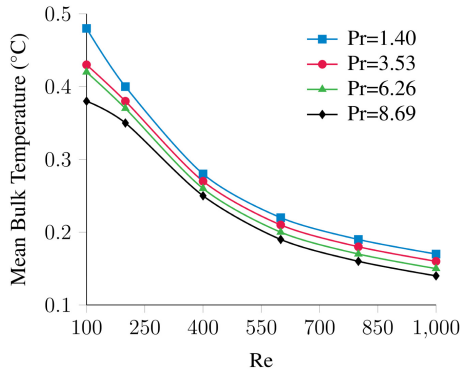


Fig. 19. (Color online) Consequences of Pr on the mean bulk temperature for parallel plate channel.

even temperature to nanoparticles in comparison to boundary value due to shooting viscous dissipation values. Higher nanofluid thermal conductivity than base fluid ($\phi = 0\%$) makes this easier. Further, fluid and particles get compressed near the heated wall and the particle distribution is made irregular and reduced. In addition, though nanofluid temperature is devalued, average heat transfer increases along the channel with the help of nanofluid.

Upon varying the influencing parameters, the mid-height horizontal velocity experienced outstanding change. The characteristic shape of wall waviness is transferred to the flow and to the U velocity profiles as evident in Figs. 20 and 21 that leads to heat transfer enhancement through the wake generation. As the Pr increases from 1.4 to 8.69, at the axial distance of 0.6, the U velocity waviness is maximum for the minimum value of Pr. Velocity field diminishes at the coordinates 0 and 1 and shows enhancement at the centerline region of the channel. There is 200% enhancement in U velocity for cylindrical wavy channel and 177% enhancement in U velocity for parallel plate wavy channel, when the Pr is increased from 1.4 to 8.69 at the central region of the channel.

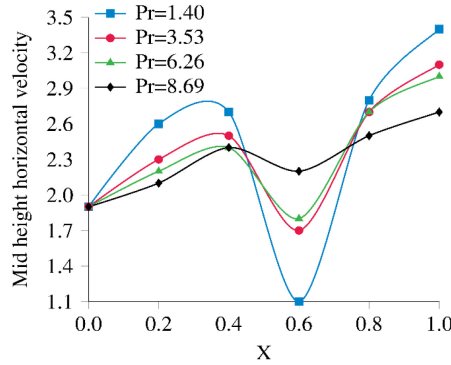


Fig. 20. (Color online) Consequences of Pr on the mid-height horizontal velocity for cylindrical channel.

The enhancement in viscous force makes the fluid velocity decelerated. Though the concentration of the flow velocity is at the channel center at the beginning, as the addition of nanoparticles increases from 0% to 4%, it distributes to the full channel domain. The fluid with lower concentration moves faster than that with higher concentration. So thermophoresis is to be controlled with an optimum lower value to get higher nanoparticle concentration adjacent to the walls. Rise in buoyancy/viscous forces causes a significant reduction in magnitude of centerline velocity in the channel (80.1% for cylindrical wavy channel and 78.17% for parallel plate wavy channel). When the concentration function of nanoparticles near the walls is decreased, Brownian motion of the nanoparticles increased. The major flow changes are limited to channel center and hot walls. The maximum horizontal velocity magnitude decreases with the enhancement in Brownian motion, increasing the temperature. The increase of thermophoresis leads to the decrease of heat transfer rate on the walls due to the effect of nanoparticle's heat capacity.

The possible reason for the higher heat transfer in the cylindrical wavy porous channel than the parallel plate wavy porous channel is due to the larger effective

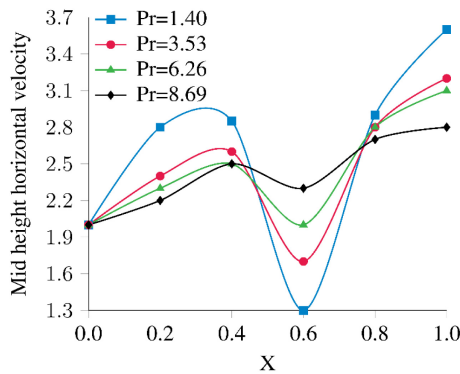


Fig. 21. (Color online) Consequences of Pr on the mid-height horizontal velocity for parallel plate channel.

surface area which was exposed to the nanofluid and the higher conduction mode of heat transfer and waviness factor associated with the cylindrical wavy channel.


5. Conclusions

A numerical study on forced convective heat transfer using Al_2O_3 -water nanofluid flow through cylindrical and parallel plate wavy porous channels subjected to the uniform wall heat flux and Buongiorno's model is carried out. In this study, thermophoresis reduced the maximum magnitudes of velocity and particle concentration, and increased the temperature profiles and pressure drop in the wavy channel. Thermophoresis has decreasing effects on the Nusselt number including the impact of Reynolds number. Variations of local density, viscosity and thermal conductivity sequentially affect the enhancement in heat transfer by nanoparticle thermophoresis. Brownian motion increases Nusselt number first, causing it to reach to a maximum value and then decrease. Brownian motion decreases concentration function near the walls while it enhances temperature and concentration fields. The Prandtl number and volume fraction account for the fluid flow structures and the temperature profile in a wavy channel and their highest values coincide with the maximum heat transfer rate and hence are geometry-dependent. Using wavy channel is a suitable method to increase the thermal performance and the compactness. The effectiveness of the cylindrical wavy channel as a heat transfer enhancement device than the parallel plate wavy porous channel is confirmed.

Acknowledgments

The authors extend their appreciation to the Deanship of Scientific Research at King Khalid University, for funding this work through Large Groups Research Project under the Grant No. RGP 2/86/44.

ORCID

M. K. Nayak  <https://orcid.org/0000-0003-0220-3760>

References

1. S. U. S. Choi, Enhancing thermal conductivity of fluids with nanoparticles, in *Proc. 1995 Int. Mechanical Engineering Congr. and Exhibition*, Vol. 231 (ASME Fluids Engineering Division, 1995), pp. 99–105.
2. K. Sadiq, I. Siddique, I. Khan, M. Ijaz Khan and A. Singh, *Int. Commun. Heat Mass Transf.* **148** (2023) 107024.
3. A. Rehman, M. Inc, B. Salah and S. Hussain, *Mod. Phys. Lett. B* **37** (2023) 2350113.
4. A. Rehman, K. Guedri, M. Inc and R. T. Alqahtani, *Mod. Phys. Lett. B* **37** (2023) 2350146.
5. F. Ahmed, *Mod. Phys. Lett. B* **37** (2023) 2350135.

6. J. A. Haider, S. Gul, K. A. Gepreel, M. N. Khan and S. A. Lone, *Mod. Phys. Lett. B* (2021), doi: 10.1142/S0217984923502445.
7. S. Hammid, K. Naima, S. Alqahtani, S. Alshehry, K. H. Oudah, O. M. Ikumapayi and Y. Menni, *Mod. Phys. Lett. B* (2021), doi: 10.1142/S0217984924500064.
8. M. K. Nayak, *Int. J. Mech. Sci.* **125** (2017) 185.
9. Y. M. Chu, M. I. Khan, N. B. Khan, S. Kadry, S. U. Khan, I. Tlili and M. K. Nayak, *Int. Commun. Heat Mass Transf.* **118** (2020) 104893.
10. M. K. Nayak, J. Prakash, D. Tripathi and V. S. Pandey, *Propuls. Power Res.* **8** (2019) 339.
11. M. K. Nayak, N. S. Akbar, D. Tripathi, Z. H. Khan and V. S. Pandey, *Adv. Powder Technol.* **28** (2017) 2159.
12. M. A. Ahmed, N. H. Shuaib and M. Z. Yusoff, *Int. J. Heat Mass Transf.* **55** (2012) 5891.
13. L. Lin, J. Zhao, G. Lu, X. D. Wang and W. M. Yan, *Int. J. Therm. Sci.* **118** (2017) 423.
14. N. Ijaz, A. Zeeshan, M. M. Bhatti and R. Ellahi, *J. Mol. Liq.* **250** (2018) 80.
15. M. Rasoulzadeh and M. Panfilov, *Phys. Fluids* **30** (2018) 106604.
16. D. D. Vo, J. Alsarraf, A. Moradikazerouni, M. Afrand, H. Salehipour and C. Qi, *Powder Technol.* **345** (2019) 649.
17. M. U. Sajid, H. M. Ali, A. Sufyan, D. Rashid, S. U. Zahid and W. U. Rehman, *J. Therm. Anal. Calorim.* **137** (2019) 1279.
18. M. S. Sadeghi, T. Tayebi, A. S. Dogonchi, M. K. Nayak and M. Waqas, *Int. Commun. Heat Mass Transf.* **120** (2021) 104951.
19. M. Hajipour and A. M. Dehkordi, *Int. J. Therm. Sci.* **55** (2012) 103.
20. J. S. K. Reddy and D. Bhargavi, Thermally developing region of a parallel plate channel partially filled with a porous material with the effect of axial conduction and viscous dissipation: Uniform wall heat flux, in *Advances in Applied Mechanical Engineering, Lecture Notes in Mechanical Engineering* (Springer, Singapore, 2020), pp. 27–35.
21. M. A. Sheremet, C. Revnic and I. Pop, *Appl. Math. Comput.* **299** (2017) 1.
22. M. Turkyilmazoglu, *Int. J. Heat Mass Transf.* **126** (2018) 974.
23. ANSYS, *ANSYS Fluent Theory Guide 15.0* (ANSYS, Inc., Canonsburg, 2013).
24. F. R. Menter, *AIAA J.* **32** (1994) 1598.
25. C. H. Li and G. P. Peterson, *J. Appl. Phys.* **101** (2007) 044312.
26. G. Tanda and G. Vittori, *Heat Mass Transf.* **31** (1996) 411.